Journal of Hazardous Materials 192 (2011) 1291–1298

Contents lists available at ScienceDirect

Journal of Hazardous Materials

journal homepage: www.elsevier.com/locate/jhazmat

Study on the interaction of phthalate esters to human serum albumin by steady-state and time-resolved fluorescence and circular dichroism spectroscopy

Xiaoyun Xie[a,c], Zhaowei Wang[c], Ximin Zhou[a], Xiaoru Wang[a], Xingguo Chen[a,b,*]

[a] National Key Laboratory of Organic Chemistry, Lanzhou University, Lanzhou 730000, China
[b] Department of Chemistry, Lanzhou University, Lanzhou 730000, China
[c] College of Earth and Environmental Sciences, Lanzhou University, Lanzhou 730000, China

ARTICLE INFO

Article history:
Received 15 February 2011
Received in revised form 12 June 2011
Accepted 14 June 2011
Available online 25 June 2011

Keywords:
Phthalate esters
Human serum albumin
Fluorescence
Molecular modelling
Circular dichroism

ABSTRACT

Phthalate esters (PAEs) are globally pervasive contaminants that are considered to be endocrine disruptor chemicals and toxic environmental priority pollutants. In this paper, the interactions between PAEs and human serum albumin (HSA) were examined by molecular modelling, steady state and time-resolved fluorescence, ultraviolet–visible spectroscopy (UV–vis) and circular dichroism spectroscopy (CD). The association constants between PAEs and HSA were determined using the Stern–Volmer and Scatchard equations. The binding of dimethyl phthalate (DMP) to HSA has a single class of binding site and its binding constants (K) are 4.08×10^3, 3.97×10^3, 3.45×10^3, and 3.20×10^3 L mol^{-1} at 289, 296, 303, and 310 K, respectively. The Stern–Volmer and Scatchard plots both had two regression curves for HSA–butylbenzyl phthalate (BBP) and HSA–di-2-ethylhexyl phthalate (DEHP), which indicated that these bindings were via two types of binding sites: the numbers of binding site for the first type were lower than for the second type. The binding constants of the first type binding site were higher than those of the second type binding site at corresponding temperatures, the results suggesting that the first type of binding site had high affinity and the second binding site involved other sites with lower binding affinity and selectivity. The thermodynamic parameters of the binding reactions (ΔG°, ΔH° and ΔS°) were measured, and they indicated the presences of hydrophobic forces and hydrogen interactions in the PAEs–HSA interactions, which agreed well with the results from molecular modelling. The alterations of protein secondary structure in the presence of PAEs were confirmed by UV–vis and CD spectroscopy. The time-resolved fluorescence study showed that the lifetime of Trp residue of HSA decreased after the addition of PAEs, which implied that the Trp residue of HSA was the main binding site.

1. Introduction

Phthalate esters (PAEs) are widely used as plasticizers in industrial processes, and as non-plasticizers in consumer products [1,2]. Due to their wide applications and growing demand, PAEs have become one of the highest yielding chemicals in the world. Nowadays their worldwide production including manufacturing of household goods amount to 6 million tones per year [3,4]. With the widespread manufacture and application of PAEs, they are inevitably discharged into environment and also have been detected in human serum and plasma [5–8]. In recent years, PAEs have attracted the interests of an increasing number of scientists since they are known with their carcinogenic, endocrine disrupting, and toxic effects on the environment and humans. In light of this negative health potential, environmental regulations have been brought to prevent the human intake of PAEs. These developments have led to an increasing interest and research effort on the effects and control of PAEs [9–11]. The affinity between PAEs and serum albumin is an important factor to understand the pharmacokinetics and pharmacodynamic properties of PAEs as it strongly influences PAEs distribution and determines the free fraction that is available for subsequent interactions with targeted receptors [12].

Human serum albumin (HSA) is the most abundant protein in plasma, which functions in the maintenance of colloid osmotic blood pressure and in the binding and transportation of various ligands such as fatty acids, hormones, and drugs, then transports them between tissues and organs [13]. It has been shown that the distribution, free concentration, and metabolism of various ligands can be significantly altered as a result of their binding to HSA [14]. Ligand interactions at the protein binding level will in most cases significantly affect the apparent distribution volume of the ligands and also affect the elimination rate of ligands. Therefore,

* Corresponding author at: Department of Chemistry, Lanzhou University, Lanzhou 730000, China. Tel.: +86 931 8912763; fax: +86 931 8912582.
E-mail address: chenxg@lzu.edu.cn (X. Chen).

0304-3894/$ – see front matter © 2011 Elsevier B.V. All rights reserved.
doi:10.1016/j.jhazmat.2011.06.038

investigating the interactions of PAEs and HSA are significant for knowing their transports and distributions in the body and clarifying their action mechanisms and pharmaceutical dynamics. As of yet, however, no work has been reported for the mechanism of these interactions and the detailed physicochemical characterizations of PAEs binding to HSA.

In this paper, we present a spectroscopic analysis of the interaction of HSA with three PAEs (structure shown in Fig. 1) such as dimethyl phthalate (DMP), butylbenzyl phthalate (BBP), and di-2-ethylhexyl phthalate (DEHP) in aqueous solution at physiological conditions, using constant protein concentration and various PAEs compositions. Structural information regarding PAEs binding mode and the effects of PAEs–HSA complexation on the protein stability and secondary structure are reported here.

2. Materials and methods

2.1. Materials

HSA (fatty acid content <0.05%) was purchased from the Sigma Chemical Company and used without further purification. Its molecular weight was assumed to be 66,478 in calculating molar concentration. HSA was dissolved under simulated physiological conditions (pH 7.40), and this stock solution (3.0×10^{-5} M) was kept in the dark at 277 K. PAEs (≥95%) were obtained from the Dr. Ehrenstorfer GmbH (Germany). Stock solutions of DMP, BBP, and DEHP were prepared at a concentration of 5.0×10^{-2}, 3.0×10^{-3}, and 2.5×10^{-2} M in absolute methanol. All other reagents were of analytical reagent grade. Ultrapure water was used throughout the experiments, and NaCl (1.0 M) solution was used to maintain the ionic strength at 0.1. Buffer solution (pH 7.40) consisted of Tris (0.2 M) and HCl (0.1 M), and the pH was adjusted to 7.40. Dilutions of the HSA stock in Tris–HCl buffer solution were prepared immediately before use. All pH values were checked with a PHS-3B acidity meter (Shanghai precision and scientific Co., Ltd.).

2.2. Apparatus and methods

The crystal structure of HSA in complex with R-warfarin was taken from the Brookhaven Protein Data Bank (entry code 1h9z) [15]. The potential of the 3D structures of HSA was assigned according to the Amber 4.0 force field with Kollman-all-atom charges. Initial structures of all molecules were generated by molecular modelling software Sybyl 6.9 [16]. The geometries of these compounds were subsequently optimised using the Tripos force field with Gasteiger–Marsili charges. The FlexX program was applied to calculate the possible conformation of the ligands that binds to the protein. Using this kind of approach, a computational model of the target receptor was built, and partial binding parameters of the PAEs–HSA system were calculated through the Sybyl 6.9 software.

Fluorescence spectra and intensities were recorded with a RF-5301PC Spectrofluorometer (Shimadzu, Japan) in a 1 cm quartz cell. Both excitation and emission bandwidths were set at 5 nm. The excitation wavelength was 280 nm, and the emission wavelength was read at 290–500 nm with a maximum observed at 334 nm.

In performing the fluorescence titration experiments, 3.0 mL of solution containing the appropriate concentration of HSA was titrated manually by the successive addition of methanol stock solutions of PAEs with trace syringes. The fluorescence intensity was subsequently measured. DMP experiments were measured at four temperatures (289, 296, 303, and 310 K). BBP and DEHP experiments were measured at three temperatures (290, 300, and 310 K). The temperature of the sample was maintained by an electronic thermo-regulating water-bath (NTT-2100, EYELA, Japan). The binding constants can be calculated by modified Stern–Volmer equation [17]:

$$\frac{F_0}{(F_0 - F)} = \frac{1}{(f\,K[Q])} + \frac{1}{f} \tag{1}$$

where F_0 is initial fluorescence intensity and F is fluorescence intensities in the presence of quenching agent (or interacting molecule). K is the Stern–Volmer quenching constant, [Q] is the molar concentration of quencher, and f is the fraction of accessible fluorophore to a polar quencher, which indicates the fractional fluorescence contribution of the total emission for an interaction with a hydrophobic quencher. The plot of $F_0/(F_0 - F)$ versus $1/[Q]$ yields f^{-1} as the intercept on y axis and $(fK)^{-1}$ as the slope. Thus, the ratio of the ordinate and the slope gives K.

The data obtained were also analyzed using Scatchard's equation to calculate binding constants and the number of binding sites [18]:

$$\frac{r}{D_f} = nK - rK \tag{2}$$

where r is the number of moles of small molecules bound per mole of protein, D_f is the molar concentration of free small molecules, n is the binding site multiplicity per class of binding site and K is the binding constant. PAEs possess intrinsic fluorescence at the λ_{ex} of HSA (280 nm). The fluorescence emission intensities of PAEs were measured at 334 nm as a blank titration series (*i.e.*, successive addition of PAEs stock solutions into 3.0 mL buffer with trace syringes) to eliminate background effects on the HSA fluorescence quenching values. The fluorescence values obtained were then subtracted from the fluorescence intensity values obtained for HSA quenching [19].

Thermodynamic parameters were calculated based on the temperature dependence of the binding constant for PAEs–HSA binding. The temperatures used were 289, 296, 303, and 310 K for DMP and 290, 300, and 310 K for BBP and DEHP. The enthalpy change (ΔH°) was calculated from the slope of the Van't Hoff relationship:

$$\ln K = \frac{-\Delta H^\circ}{RT} + \frac{\Delta S^\circ}{R} \tag{3}$$

where K is the binding constant at temperature, T is temperature and R is the ideal gas constant. The value of ΔS° was also obtained from the linear Van't Hoff plot. Consequently, the value of ΔG° was able to be calculated from the equation:

$$\Delta G^\circ = \Delta H^\circ - T\Delta S^\circ \tag{4}$$

Time-resolved fluorescence spectra were executed in a time-correlated single photon counting system from FL920P spectro-meter (Edinburgh Instruments, UK) with λ_{ex} = 295 nm. The data are fitted to triexponential functions after deconvolution of the instrumental response function by an iterative reconvolution approach by the DAS6 decay analysis software utilizing reduced χ^2 and weighted residuals as parameters for goodness of fit. Average fluorescence lifetime (τ) for triexponential iterative fittings was calculated from the decay times and the normalized preexponential factors using the following equation:

$$\langle\tau\rangle = \frac{\sum \alpha_i \tau^2}{\sum \alpha_i \tau} \tag{5}$$

UV–vis spectroscopy was performed on a Shimadzu UV-240 at 298 K from 190–350 nm using a quartz cuvette with 1 cm path length.

CD spectral measurements were run on an Olis DSM 1000 (USA) automatic recording spectrophotometer in a 1 mm cell under nitrogen atmosphere. The slit width was set at 5 nm, and the speed

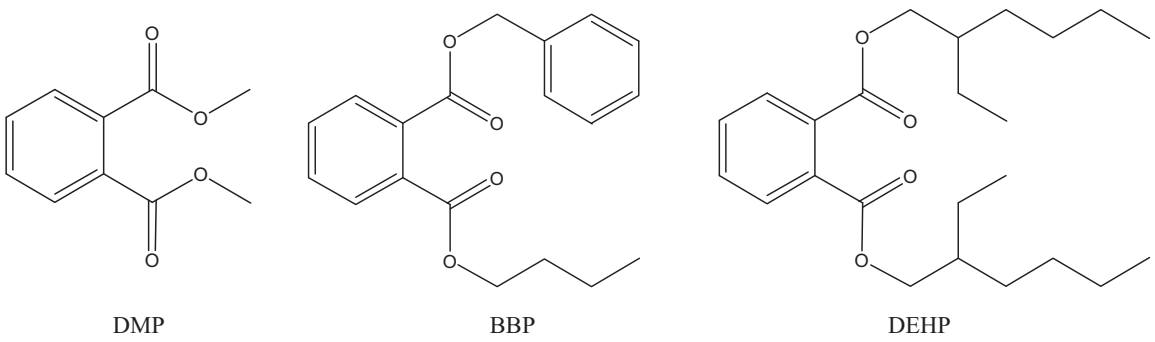

Fig. 1. The chemical structures of PAEs.

of scanning was 30 nm min^{-1}. Each spectrum represents the average of five successive scans. CD spectra (200–350 nm) were taken at HSA concentrations of 3.0×10^{-6} M, spectra were corrected for buffer signal, and conversion to the Mol CD ($\Delta\varepsilon$) was performed with the Jasco Standard Analysis software. The protein secondary structure was calculated using SELCON3, The program SELCON3 is provided in CDPro software package.

3. Results and discussion

3.1. Molecular modelling study of the interaction between PAEs and HSA

Molecular modelling was carried out using the Sybyl 6.9 software to investigate whether PAEs bind to HSA. Descriptions of 3D structure of crystalline albumin have revealed that human serum albumin comprises of three homologous α-helical domains (I–III): I (residues 1–195), II (196–383), III (384–585), that assemble to form a heart-shaped molecule. Each domain has two subdomains (A and B), which are six (A) and four (B) α-helices, respectively [20].

Aromatic and heterocyclic ligands have been found to bind within two hydrophobic pockets, called site I and site II, in sub domains IIA and IIIA [21]. The sole tryptophan residue (Trp-214) of HSA is in sub-domain IIA. There is a large hydrophobic cavity present in sub-domain IIA that many small molecules can bind to. The binding modes between the three PAEs and HSA are shown in Fig. 2(A–C). The docking results showed that DMP, BBP and DEHP were all located within the binding pocket of subdomain IIA (The Warfarin Binding Pocket). It is important to note that Trp-214 was positioned close to PAEs, which suggests the existence of hydrophobic interactions between them. Additionally, this phenomenon provided a good structural basis to explain the very efficient fluorescence quenching of HSA emission in the presence of PAEs. On the other hand, there were hydrogen bonds between the –O of DMP and the Arg-222 residue of HSA and between the –O of DMP and the Leu-238 residue. For BBP, there were hydrogen bonds between the –O of BBP and the Arg-222 residue of HSA and between the –O of BBP and the Val-216 residue. For DEHP, there were hydrogen bonds between the –O of DEHP and the Arg-222 residue of HSA and between the –O of DEHP and the Leu-260 residue. These results indicated that the formation of hydrogen bonds decreased the hydrophilicity of the three PAEs and increased their hydrophobicity, which made the PAEs–HSA system stable. The calculated binding Gibbs free energy (ΔG°) was −18.78, −19.80, −11.37 kJ mol^{-1} for DMP, BBP and DEHP respectively. The results obtained from the modelling suggested that the interaction between the three PAEs and HSA was dominated by hydrophobic forces and also showed the existence of hydrogen bonds. Spectral methods were thus employed to obtain information related to the binding mechanisms of the three PAEs to HSA and substantiate the results from molecular modelling.

3.2. Analysis of fluorescence quenching of HSA by PAEs

Fluorescence spectroscopy is widely employed to study proteins and peptides. The intrinsic fluorescence of HSA is very sensitive to its microenvironment. Actually, the intrinsic fluorescence of HSA is almost contributed by tryptophan alone, because phenylalanine has a very low quantum yield and the fluorescence of tyrosine is almost totally quenched if it is ionized or near an amino group, a carboxyl group, or a tryptophan [22]. When local surroundings of HSA were altered slightly its intrinsic fluorescence would weaken obviously, such factors as protein conformational transition, biomolecule binding, and denaturation, etc. are responsible for the weakening. Fig. 3(A–C) showed the fluorescence emission spectra (λ_{ex} = 280 nm) obtained for HSA at pH 7.40 with the addition of three PAEs compounds. These were corrected by subtracting the spectra of free PAEs from the quenching spectra as described earlier. This mode of correction has already been validated [19,23].

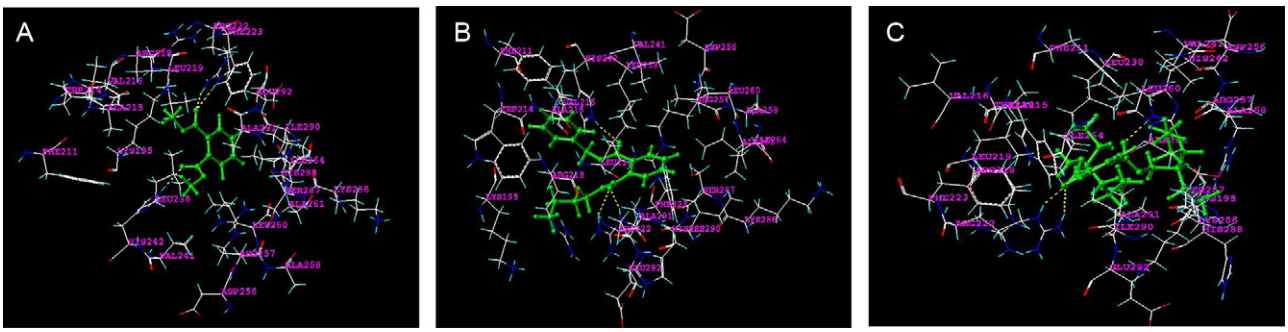

Fig. 2. The interaction model between PAEs and HSA, only residues around 6.5 Å of the ligand are displayed. The residues of HSA are represented using line and the PAEs structure is represented using ball and stick model. The hydrogen bond between PAEs and HSA is represented by yellow dashed line. (A) HSA–DMP. (B) HSA–BBP. (C) HSA–DEHP. (For interpretation of the references to color in this figure legend, the reader is referred to the web version of the article.)

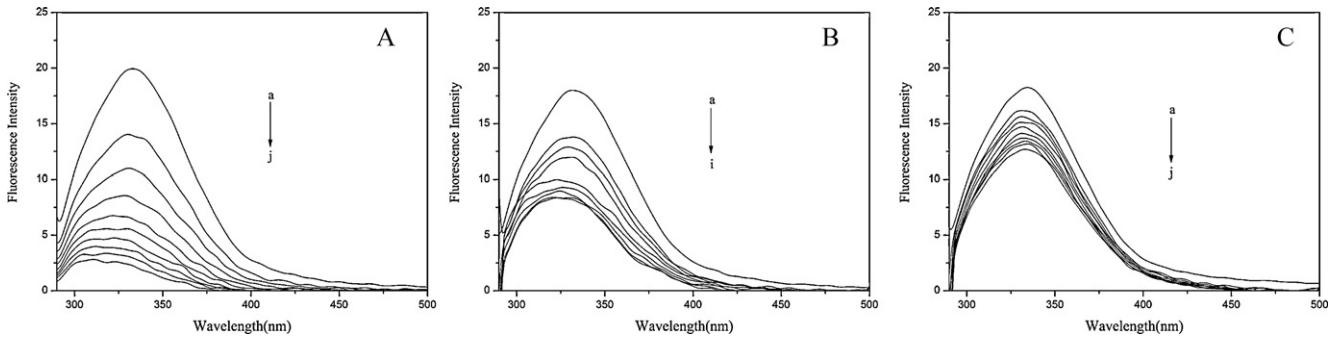

Fig. 3. Corrected HSA fluorescence emission spectra with the subtraction of PAEs emission spectra at the appropriate concentration and same λ_{ex}. (A) The concentration of HSA was 3.0×10^{-6} M while the DMP concentration corresponding to 0, 8.3×10^{-5}, 1.7, 2.5, 3.3, 4.2, 5.0, 5.8, 6.7 and 7.5×10^{-4} M from (a to j); T = 296 K; pH 7.40; λ_{ex} = 280 nm, λ_{em} = 334 nm. (B) The concentration of HSA was 3.0×10^{-6} M while the BBP concentration corresponding to 0, 5.0×10^{-6}, 1.1, 1.6, 2.1, 2.7, 3.2, 3.7 and 4.3×10^{-5} M from (a to i); T = 296 K; pH 7.40; λ_{ex} = 280 nm, λ_{em} = 334 nm. (C) The concentration of HSA was 3.0×10^{-6} M while the DEHP concentration corresponding to 0, 4.3×10^{-5}, 8.7×10^{-5}, 1.3, 1.7, 2.2, 2.6, 3.0, 3.5 and 3.9×10^{-4} M from (a to j); T = 296 K; pH 7.40; λ_{ex} = 280 nm, λ_{em} = 334 nm.

It can be seen from Fig. 3 that the fluorescence intensity of HSA decreased in the presence of three PAEs. The results indicated that the binding of the three PAEs and HSA quenched the intrinsic fluorescence of the HSA, which was in agreement with the results obtained by molecular modelling.

3.3. Binding constant and number of binding sites

Fluorescence quenching can be dynamic, resulting from collisional encounters between the fluorophore and the quencher, or static, resulting from the formation of a ground-state complex between the fluorophore (protein) and the quencher. In both cases, molecular contact is required between the fluorophore and the quencher for fluorescence quenching to occur [23]. Dynamic and static quenching can be distinguished by their difference depending on temperature [24]. Higher temperature results in faster diffusion and larger amounts of collisional quenching. This will typically lead to the dissociation of weakly bound complexes. Therefore, the quenching constant increases with the increase in temperature for dynamic quenching. It decreases, however, with increasing temperature for static quenching. The possible quenching mechanism can be interpreted by fluorescence quenching spectra of the protein and the modified Stern–Volmer curves of the three PAEs with HSA at different temperatures as shown in Fig. 4(A–C). It can be seen in Fig. 4A that the Stern–Volmer plots for the HSA–DMP were linear. In Fig. 4B and C, the Stern–Volmer plots for the HSA–BBP and HSA–DEHP at three different temperatures had no single linear relationship but had two regression curves, which suggested there were two types of binding sites in the interactions of BBP and DEHP with HSA. The binding constants calculated from the Stern–Volmer equation were listed in Table 1.

Quenching data were also analyzed using the Scatchard plot, the results (K, n) were summarised in Table 1. It can be seen in Fig. 5A that the Scatchard plots for the HSA–DMP were linear and the slopes decreased with increasing temperature, which is consistent with the static type of quenching mechanism. In Fig. 5B and C, the Scatchard plots for the HSA–BBP and HSA–DEHP at three different temperatures also had two regression curves. It can be seen from Table 1, the binding constants determined from Stern–Volmer equation were similar to the constants from Scatchard equation. The number of binding sites for the HSA–DMP, HSA–BBP and HSA–DEHP were obtained from Scatchard equation. The linearity of Stern–Volmer and Scatchard indicated that DMP could bind to one class of sites on HSA, which was in agreement with the number of binding site n in some degree; We can see that the number of binding sites (n_1 and n_2) for the HSA–BBP and HSA–DEHP were lower than 1, which implied that BBP and DEHP were only partially bound to HSA. This may be due to the long hydrophobic chains of BBP and DEHP, only a portion of them entered into the hydrophobic cavity of HSA, so the corresponding number of binding sites decreased. Moreover, the binding constants K_2 were lower than K_1 at corresponding temperatures. The results indicated that at low concentration, the first type of binding site had high affinity, while at high concentration, BBP and DEHP involved other sites with lower binding affinity and selectivity, accordingly resulting in the decrease in binding constants [17,25]. The order of binding affinity of HSA for all test phthalates is: BBP > DEHP > DMP. PAEs are known as liposoluble compounds, which are lipophilic enough to insert into the hydrophobic cavity of HSA in aqueous solution. Alco-

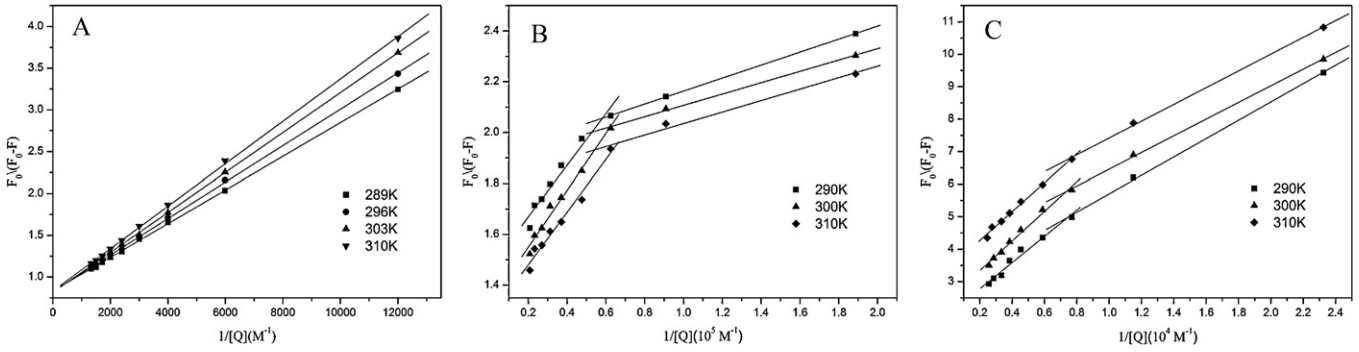

Fig. 4. The modified Stern–Volmer plot for the HSA–PAEs systems at different temperatures. (A) [HSA] = 3.0×10^{-6} M; [DMP] = 8.3×10^{-5}, 1.7, 2.5, 3.3, 4.2, 5.0, 5.8, 6.7 and 7.5×10^{-4} M; pH 7.40; λ_{ex} = 280 nm, λ_{em} = 334 nm. (B) [HSA] = 3.0×10^{-6} M; [BBP] = 5.0×10^{-6}, 1.1, 1.6, 2.1, 2.7, 3.2, 3.7, 4.3 and 4.8×10^{-5} M; pH 7.40; λ_{ex} = 280 nm, λ_{em} = 334 nm. (C) [HSA] = 3.0×10^{-6} M; [DEHP] = 4.3×10^{-5}, 8.7×10^{-5}, 1.3, 1.7, 2.2, 2.6, 3.0, 3.5 and 3.9×10^{-4} M; pH 7.40; λ_{ex} = 280 nm, λ_{em} = 334 nm.

Table 1
Binding parameters for the interaction of the HSA and PAEs.

	T (K)	Modified Stern–Volmer		Scatchard			
		K_1 (M^{-1})	K_2 (M^{-1})	K_1 (M^{-1})	K_2 (M^{-1})	n_1	n_2
HSA–DMP	289	4.14×10^3		4.08×10^3		1.21	
	296	3.80×10^3		3.97×10^3		1.19	
	303	3.42×10^3		3.45×10^3		1.22	
	310	3.28×10^3		3.20×10^3		1.22	
HSA–BBP	290	7.60×10^5	1.45×10^5	7.45×10^5	1.32×10^5	0.52	0.69
	300	7.89×10^5	1.27×10^5	7.60×10^5	1.19×10^5	0.53	0.76
	310	8.18×10^5	1.19×10^5	7.69×10^5	1.13×10^5	0.55	0.79
HSA–DEHP	290	1.23×10^4	4.88×10^3	1.10×10^4	4.32×10^3	0.34	0.54
	300	1.52×10^4	3.91×10^3	1.29×10^4	3.38×10^3	0.27	0.57
	310	1.87×10^4	3.05×10^3	1.54×10^4	2.96×10^3	0.22	0.52

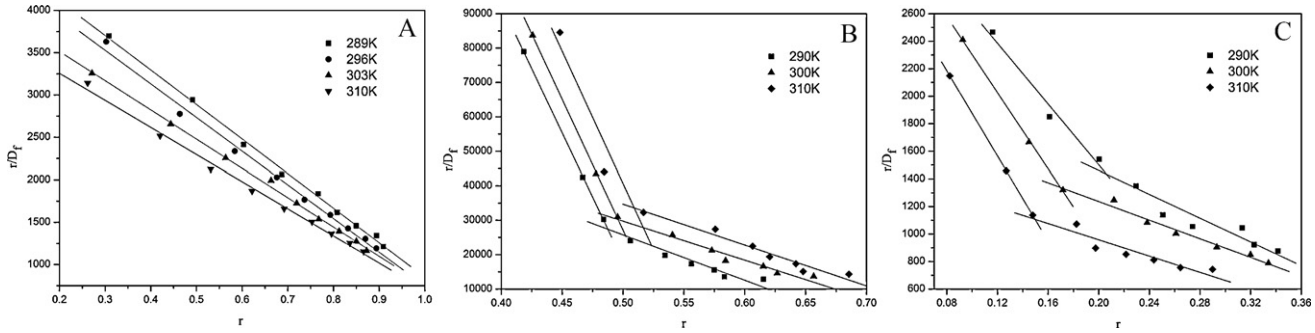

Fig. 5. The Scatchard plot for the HSA–PAEs systems at different temperatures. (A) [HSA] = 3.0×10^{-6} M; [DMP] = 8.3×10^{-5}, 1.7, 2.5, 3.3, 4.2, 5.0, 5.8, 6.7 and 7.5×10^{-4} M; pH 7.40; λ_{ex} = 280 nm, λ_{em} = 334 nm. (B) [HSA] = 3.0×10^{-6} M; [BBP] = 5.0×10^{-6}, 1.1, 1.6, 2.1, 2.7, 3.2, 3.7, 4.3 and 4.8×10^{-5} M; pH 7.40; λ_{ex} = 280 nm, λ_{em} = 334 nm. (C) [HSA] = 3.0×10^{-6} M; [DEHP] = 4.3×10^{-5}, 8.7×10^{-5}, 1.3, 1.7, 2.2, 2.6, 3.0, 3.5 and 3.9×10^{-4} M; pH 7.40; λ_{ex} = 280 nm, λ_{em} = 334 nm.

hol parts of the DMP and DEHP are fatty chain, the general trends increasing binding strength with increasing fatty chain lengths is similar both to the chain-length dependence of hydrophobicity. Alcohol part of the BBP contains a benzene ring, it seems more hydrophobic. So HSA–BBP exhibited higher affinity as compared to HSA–DMP and HSA–DEHP at all temperature.

3.4. Thermodynamic analysis and the nature of the binding forces

Considering the dependence of binding constant on temperature, a thermodynamic process was considered to be responsible for the formation of the complex [14,26]. Therefore, the dependences of thermodynamic parameters on the temperature were analyzed to further characterize the acting forces between the three PAEs and HSA. The interaction forces between small molecules and biomolecules may include electrostatic interactions, multiple hydrogen bonds, van der Waals interactions, and hydrophobic and steric contacts within the antibody-binding site. The thermodynamic parameters, enthalpy (ΔH°) and entropy (ΔS°) of reaction are the main evidence for confirming the binding force. The values of ΔH° and ΔS° can be obtained from the linear relationship between $\ln K$ and the reciprocal of absolute temperature, and the results were presented in Table 2. It was clear from the values of standard entropy changes (ΔS°) and standard enthalpy changes (ΔH°) that binding of the three PAEs to HSA occur thru endothermic processes accompanied by positive values of ΔS° and negative values of ΔG°. The binding processes are always spontaneous as evidenced by the negative sign of ΔG° values. The positive entropy changes arised from water molecules arranged more random around HSA and the three PAEs, caused by hydrophobic interactions between HSA and PAEs molecules. For DMP, The negative ΔH° value (-9.22 kJ mol^{-1}) observed can not be mainly attributed to electrostatic interactions since for electrostatic interactions ΔH° is very small, almost zero [27,28]. Negative ΔH° value is observed whenever there is hydrogen bonding in the binding. The negative ΔH° and positive ΔS° values, therefore, showed that

Table 2
Thermodynamic parameters for the interaction of the HSA and PAEs.

	T (K)	ΔG° (kJ mol^{-1})		ΔS° (J mol^{-1} K^{-1})		ΔH° (kJ mol^{-1})	
		n_1	n_2	n_1	n_2	n_1	n_2
HSA–DMP	289	−20.03		37.42		−9.22	
	296	−20.29					
	303	−20.55					
	310	−20.82					
HSA–BBP	290	−32.60	−28.41	116.56	78.23	1.20	−5.72
	300	−33.77	−29.19				
	310	−34.93	−29.97				
HSA–DEHP	290	−22.43	−20.15	120.48	20.48	12.51	−14.21
	300	−23.64	−20.35				
	310	−24.84	−20.56				

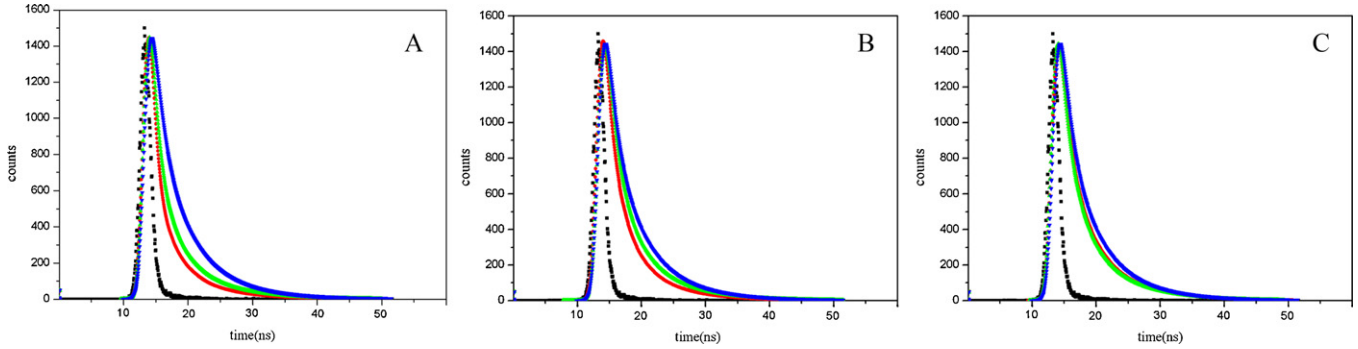

Fig. 6. The time-resolved fluorescence decay of HSA–PAEs systems. (A) 3.0×10^{-6} M HSA is represented by blue dotted line; 3.0×10^{-6} M HSA + 8.3×10^{-5} M DMP is represented by green dotted line; 3.0×10^{-6} M HSA + 1.7×10^{-4} M DMP is represented by red dotted line; Instrument response is represented by black dotted line. (B) 3.0×10^{-6} M HSA is represented by blue dotted line; 3.0×10^{-6} M HSA + 5.0×10^{-6} M BBP is represented by green dotted line; 3.0×10^{-6} M HSA + 1.1×10^{-5} M BBP is represented by red dotted line; Instrument response is represented by black dotted line. (C) 3.0×10^{-6} M HSA is represented by blue dotted line; 3.0×10^{-6} M HSA + 4.3×10^{-5} M DEHP is represented by green dotted line; 3.0×10^{-6} M HSA + 8.7×10^{-5} M DEHP is represented by red dotted line; Instrument response is represented by black dotted line. (For interpretation of the references to color in this figure legend, the reader is referred to the web version of the article.)

Table 3
Fluorescence decay fitting parameters for the interaction of the HSA and PAEs.

	HSA	HSA–DMP		HSA–BBP		HSA–DEHP	
	3.0×10^{-6} M	$+8.3 \times 10^{-5}$ M	$+1.7 \times 10^{-4}$ M	$+5.0 \times 10^{-6}$ M	$+1.1 \times 10^{-5}$ M	$+4.3 \times 10^{-5}$ M	$+8.7 \times 10^{-5}$ M
τ_1 (ns)	1.33	0.51	0.47	1.27	0.55	0.84	0.58
α_1	0.21	0.24	0.37	0.26	0.17	0.16	0.13
τ_2 (ns)	4.20	2.33	2.51	3.65	2.17	2.73	2.34
α_2	0.47	0.33	0.31	0.42	0.42	0.36	0.37
τ_3 (ns)	8.04	6.52	6.56	7.60	6.24	6.63	6.49
α_3	0.32	0.44	0.32	0.32	0.41	0.49	0.50
χ^2	1.11	1.07	1.01	1.08	1.05	1.08	1.04
$\langle\tau\rangle$ (ns)	6.08	5.47	5.19	5.71	5.05	5.58	5.53

both hydrogen bond and hydrophobic interactions play a role in the binding of DMP to HSA. For BBP and DEHP, the first types of binding sites had both positive ΔH° and ΔS° values, which were typical of hydrophobic interactions. Negative ΔH° values are observed both in the second type of binding site for the interactions between BBP, DEHP and HSA indicated that hydrogen interactions might play major roles.

3.5. Time-resolved fluorescence spectra

Time-resolved fluorescence measurements can give information about the conformational heterogeneity of proteins. In order to further substantiate the quenching mechanism of the three PAEs to HSA, fluorescence lifetime of the tryptophan of HSA were ascertained in the absence and presence of the three PAEs. The fluorescence decay of the PAEs–HSA system were shown in Fig. 6(A–C) and Table 3. Fig. 6(A–C) reveals the time-resolved fluorescence decays of HSA in Tris–HCl buffer at pH7.40. The data required three exponentials to obtain an adequate fit with the χ^2 for individual data curves ranging from 1.0 to 1.1. The lifetime components (τ_i) of HSA alone were 1.33 ns, 4.20 ns, and 8.04 ns, with associated fractional intensities (α_i) 0.21, 0.47, 0.32, respectively (Table 3). As the three PAEs were added to HSA, τ_1, τ_2 and τ_3 were all decreased. The observed decreases in the average lifetime of the tryptophan of HSA as the concentration of the three PAEs was increased were also consistent with the quenching of the intensity by the three PAEs. Therefore, the binding of the three PAEs to HSA results in the more hydrophobic environment of Trp residue of HSA, which was in agreement with the results of steady state fluorescence studies [29,30].

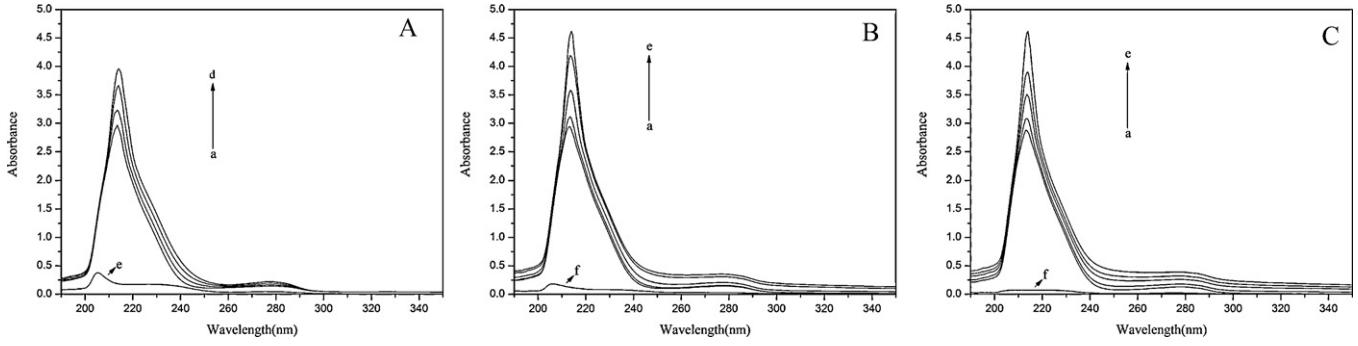

Fig. 7. UV absorbance spectra of HSA. (A) HSA concentration was at 3.0×10^{-6} M (a) and DMP concentration for HSA–DMP system was at 8.0×10^{-5}, 1.7, 2.5×10^{-4} M (b–d). A concentration of 8.0×10^{-5} M DMP (e) was used for DMP only, pH 7.40, T = 298 K. (B) HSA concentration was at 3.0×10^{-6} M (a) and BBP concentration for HSA–BBP system was at 5.0×10^{-6}, 1.1, 1.6, 2.1×10^{-5} M (b–e). A concentration of 5.0×10^{-6} M BBP (f) was used for BBP only, pH 7.40, T = 298 K. (C) HSA concentration was at 3.0×10^{-6} M (a) and DEHP concentration for HSA–DEHP system was at 4.3×10^{-5}, 8.7×10^{-5}, 1.3, 1.7×10^{-4} M (b–e). A concentration of 4.3×10^{-5} M DEHP (f) was used for DEHP only, pH 7.40, T = 298 K.

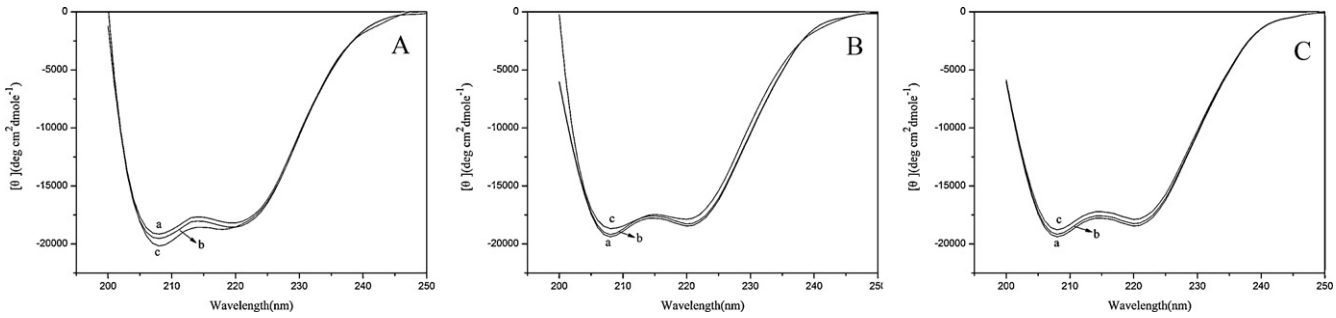

Fig. 8. CD spectra of the HSA–PAEs systems. (A) (a) 3.0×10^{-6} M HSA; (b) 3.0×10^{-6} M HSA + 4.5×10^{-5} M DMP; (c) 3.0×10^{-6} M HSA + 9.0×10^{-5} M DMP; pH 7.40, T = 298 K. (B) (a) 3.0×10^{-6} M HSA; (b) 3.0×10^{-6} M HSA + 1.9×10^{-5} M BBP; (c) 3.0×10^{-6} M HSA + 2.9×10^{-5} M BBP; pH 7.40, T = 298 K. (C) (a) 3.0×10^{-6} M HSA; (b) 3.0×10^{-6} M HSA + 4.5×10^{-5} M DEHP; (c) 3.0×10^{-6} M HSA + 9.0×10^{-5} M DEHP; pH 7.40, T = 298 K.

Table 4
Secondary structure of HSA complexes (CD Spectra) with PAEs at pH 7.40. Calculated by SELCON3 software.

	HSA	HSA–DMP		HSA–BBP		HSA–DEHP	
	3.0×10^{-6} M	$+4.5 \times 10^{-5}$ M	$+9.0 \times 10^{-5}$ M	$+1.9 \times 10^{-5}$ M	$+2.9 \times 10^{-5}$ M	$+4.5 \times 10^{-5}$ M	$+9.0 \times 10^{-5}$ M
α-Helix (%)	51.6	52.9	55.2	50.4	47.8	49.2	46.5
β-Sheet (%)	8.9	7.4	5.3	9.2	10.6	9.6	10.8
Turn (%)	15.6	16.0	16.2	15.9	16.7	16.1	17.4
Random (%)	23.9	23.7	23.3	24.5	24.9	25.1	25.3

3.6. Alterations of protein secondary structure induced by PAEs binding

In order to gain better understandings in physicochemical properties of the three PAEs governing their spectral behaviors and to draw relevant conclusions on the HSA–PAEs binding mechanisms, UV and CD spectroscopic measurements were performed on HSA and the HSA–PAEs complexes. UV–vis absorption measurement is a very simple method that is applicable to explore the structural changes and know when complex formation occurs. We measured the UV–vis absorbance spectra of HSA with various amounts of PAEs to verify the structural changes of HSA when exposed to PAEs. Fig. 7(A–C) displayed the UV–vis absorption spectra of HSA from 190 to 350 nm in buffer solution in the presence of different PAEs concentrations. The absorption of HSA at 210 nm represents the content of α-helix structure of the protein [31]. As shown in Fig. 7(A–C), HSA has a strong absorbance with a peak at 212 nm. The peak intensity increased with the addition of three PAEs compounds, and there are slight shifts of the HSA–PAEs spectra toward longer wavelengths. These changes reasonably account for the interactions of the three PAEs with HSA.

CD spectroscopy is a quantitative technique to investigate the conformation of proteins in aqueous solution. A high content of α-helices in HSA was revealed by the two minima around 208 and 222 nm. The reasonable explanation is that the negative peaks between 208 and 209 nm and 222–223 nm are both contributed to an $n \rightarrow \pi^*$ transfer for the peptide bond within an α-helix [32]. The CD spectrum of HSA in the absence and presence of different PAEs with varying concentrations were shown in Fig. 8(A–C). Secondary structure analysis based on CD results suggested that free HSA had a high α-helix content (51.6%), with 8.9% β-sheet, 15.6% turn, and 23.9% random (Fig. 8(A–C) and Table 4). Upon PAEs complexation, minor changes exhibited an increase of α-helical structures for HSA–DMP complexes accompanied by the decreasing content of β-sheet structures of HSA. However, reductions of α-helix occurred for HSA–BBP and HSA–DEHP complexes in favor of an increase in β-sheet, turn, and random coil structures. The conformational changes observed via CD results indicated that DMP stabilized protein conformation in some degree, while BBP and DEPH induced protein destabilization and unfolding partially.

4. Conclusions

The interactions between PAEs and HSA have been investigated by molecular modelling, steady state and time-resolved fluorescence, UV and CD spectroscopy. The linearity of modified Stern–Volmer and Scatchard plots indicated that DMP could bind to one class of sites on HSA, which was in agreement with the number of binding site n in some degree; While the modified Stern–Volmer and Scatchard plots for the HSA–BBP and HSA–DEHP showed that these bindings were via two types of binding sites: one with a high affinity but relatively fewer binding number and the other with a lower binding constant but greater binding number. The thermodynamic parameters of the binding reactions indicated the presences of hydrophobic forces and hydrogen interactions in the PAEs–HSA interactions, and docking calculations found the three PAEs to be located in the hydrophobic pocket of HSA within subdomain IIA. Additionally, results showed that the binding of the three PAEs to HSA induced small conformational changes in the overall structure of HSA, which was further proved by the quantitative analysis data of the UV–vis and CD spectra.

According to experimental results, the three PAEs could bind with HSA during transport and metabolic processes in vitro. This will provide important insight into the interactions of the physiologically important protein HSA with globally pervasive contaminants PAEs.

Acknowledgement

This work was kindly supported by the National Natural Science Foundation of China (No. 20875040, J0730425).

References

[1] F. Zeng, J.X. Wen, K.Y. Cui, L.N. Wu, M. Liu, Y.J. Li, Y.J. Lin, F. Zhu, Z.L. Ma, Z.X. Zeng, Seasonal distribution of phthalate esters in surface water of the urban lakesin the subtropical city, Guangzhou, China, J. Hazard. Mater. 169 (2009) 719–725.

[2] C.A. Staples, D.R. Peterson, T.F. Parkerton, W.J. Adams, The environmental fate of phthalate esters: a literature review, Chemosphere 35 (1997) 667–749.
[3] C.E. Mackintosh, J.A. Maldonado, M.G. Ikonomou, F.A.P.C. Gobas, Sorption of phthalate esters and PCBs in a marine ecosystem, Environ. Sci. Technol. 40 (2006) 3481–3488.
[4] C.J. Salima, S.H. Liua, J.F. Kennedy, Comparative study of the adsorption on chitosan beads of phthalate esters and their degradation products, Carbohydr. Polym. 81 (2010) 640–644.
[5] J.D. Blair, M.G. Ikonomou, B.C. Kelly, B. Surridge, A.P.C. Frank, F.A.P.C. Gobas, Ultra-trace determination of phthalate ester metabolites in seawater, sediments, and biota from an urbanized marine inlet by LC/ESI-MS/MS, Environ. Sci. Technol. 43 (2009) 6262–6268.
[6] B. Xu, N.Y. Gao, H.F. Cheng, S.J. Xia, M. Rui, D.D. Zhao, Oxidative degradation of dimethyl phthalate (DMP) by UV/H_2O_2 process, J. Hazard. Mater. 162 (2009) 954–959.
[7] Z.W. Xu, W.M. Zhang, L. Lv, B.C. Pan, P. Lan, Q.X. Zhang, A new approach to catalytic degradation of dimethyl phthlate by a macroporous OH-type strongly basic anion exchange resin, Environ. Sci. Technol. 44 (2010) 3130–3135.
[8] T. Suzuki, K. Yaguchi, S. Suzuki, Monitoring of phthalic acid monoesters in river water by solid-phase extraction and GC–MS determination, Environ. Sci. Technol. 35 (2001) 3757–3763.
[9] S.Y. Yuan, I.C. Huang, B.V. Chang, Biodegradation of dibutyl phthalate and di-(2-ethylhexyl) phthalate and microbial community changes in mangrove sediment, J. Hazard. Mater. 184 (2010) 826–831.
[10] US EPA, Exposure and risk assessment for phthalate esters: di(2-ethylhexyl) phthalate, di-n-butyl phthalate, dimethyl phthalate, diethyl phthalate, din-octyl phthalate, butyl benzyl phthalate, Final Report, US Environmental Protection Agency, EPA-440/4-81-020, 1981b,Washington, DC, 1981.
[11] I. Kabdaşh, A. Keleş, T. Ölmez-Hancı, O. Tünay, I. Arslan-Alaton, Treatment of phthalic acid esters by electrocoagulation with stainless steel electrodes using dimethyl phthalate as a model compound, J. Hazard. Mater. 171 (2009) 932–940.
[12] Y.J. Hu, Y. Liu, X.H. Xiao, Investigation of the interaction between berberine and human serum albumin, Biomacromolecules 10 (2009) 517–521.
[13] G. Zolese, G. Falcioni, E. Bertoli, R. Galeazzi, M. Wozniak, Z. Wypych, E. Gratton, A. Ambrosini, Steady-state and time resolved fluorescence of albumins interacting with N-Oleylethanolamine, a component of the endogenous N-Acylethanolamines, Proteins: Struct. Funct. Genet. 40 (2000) 39–48.
[14] A. Divsalar, M.J. Bagheri, A.A. Saboury, H. Mansoori-Torshizi, M. Amani, Investigation on the interaction of newly designed anticancer Pd(II) complexes with different aliphatic tails and human serum albumin, J. Phys. Chem. B 113 (2009) 14035–14042.
[15] I. Petitpas, A.A. Bhattacharya, S. Twine, M. East, S. Curry, Crystal structure analysis of warfarin binding to human serum albumin – Anatomy of drug site I, J. Biol. Chem. 276 (2001) 22804–22809.
[16] G. Morris, SYBYL Software, Version 6.9, Tripos Associates Inc., St. Louis, 2002.
[17] J.R. Lakowicz, Principles of Fluorescence Spectroscopy, 2nd ed, Kluwer/Plenum, New York, 1999.
[18] G. Scatchard, N.Y. Ann, The attraction of proteins for small molecules, Acad. Sci. 51 (1949) 660–672.
[19] A. Papadopoulou, R.J. Green, R.A. Frazier, Interaction of flavonoids with bovine serum albumin: a fluorescence quenching study, J. Agric. Food Chem. 53 (2005) 158–163.
[20] I. Sjoholm, B. Ekman, A. Kober, Binding of drugs to human serum albumin: XI. The specificity of three binding sites as studied with albumin immobilized in microparticles, Mol. Pharmacol. 16 (1979) 767–777.
[21] E. Froehlich, J.S. Mandeville, C.J. Jennings, R. Sedaghat-Herati, H.A. Tajmir-Riahi, Dendrimers bind human serum albumin, J. Phys. Chem. B. 113 (2009) 6986–6993.
[22] A. Sulkowska, Interaction of drugs with bovine and human serum albumin, J. Mol. Struct. 614 (2002) 227–232.
[23] S. Soares, N. Mateus, V.D. Freitas, Interaction of different polyphenols with bovine serum albumin (BSA) and human salivary α-amylase (HSA) by fluorescence quenching, J. Agric. Food Chem. 55 (2007) 6726–6735.
[24] G.Z. Chen, X.Z. Huang, J.G. Xu, Z.Z. Zheng, Z.B. Wang, The Methods of Fluorescence Analysis, Science Press, Beijing, 1990.
[25] C. Bertucci, E. Domenici, Reversible and covalent binding of drugs to human serum albumin: methodological approaches and physiological relevance, Curr. Med. Chem. 9 (2002) 1463–1481.
[26] R. Ambrosetti, R. Bianchini, S. Fischella, M. Fichera, M. Zandomeneghi, Resolution of the absorbance and CD spectra and formation constants of the complexes between human serum albumin and methyl orange, Chem. Eur. J. 2 (1996) 149–156.
[27] M.H. Rahman, T. Maruyama, T. Okada, K. Yamasaki, M. Otagiri, Study of interaction of carprofen and its enantiomers with human serum albumin-I: mechanism of binding studied by dialysis and spectroscopic methods, Biochem. Pharmacol. 46 (1993) 1721–1731.
[28] P.D. Ross, S. Subramanian, Thermodynamics of protein association reactions: forces contributing to stability, Biochemistry 20 (1981) 3096–3102.
[29] K.M. Hirshfield, D. Toptygin, G. Grandhige, H. Kim, B.Z. Packard, L. Brand, Steady-state and time-resolved fluorescence measurements for studying molecular interactions: interaction of a calcium-binding probe with proteins, Biophys. Chem. 62 (1996) 25–38.
[30] K. Flora, J.D. Brennan, G.A. Baker, M.A. Doody, F.V. Bright, Unfolding of acrylodan-labeled human serum albumin probed by steady-state and time-resolved fluorescence methods, Biophys. J. 75 (1998) 1084–1096.
[31] O.S. Wolfbeis, M. Leiner, P. Hochmuth, H. Geiger, Absorption and fluorescence spectra, p*Ka* values, and fluorescence lifetimes of monohydroxyflavones and monomethoxyflavones, Ber. Bunsenge. Phys. Chem. 88 (1984) 759–767.
[32] P. Yang, F. Gao, The Principle of Bioinorganic Chemistry, Science Press, 2002, p. 349.